arXiv:1704.02678v1 [cond-mat.stat-mech] 10 Apr 2017

Lyapunov Exponent and Criticality in the Hamiltonian Mean Field Model

L. H. Miranda Filho

Departamento de Física, Universidade Federal Rural de Pernambuco, Rua Manoel de Medeiros, s/n - Dois Irmãos, 52171-900 - Recife, Brazil

M. A. Amato and T. M. Rocha Filho*

Instituto de Física and International Center for Condensed Matter Physics, Universidade de Brasília, CP 04455, 70919-970 - Brasília, Brazil

Abstract

We investigate the dependence of the largest Lyapunov exponent of a N-particle self-gravitating ring model at equilibrium with respect to the number of particles and its dependence on energy. This model has a continuous phase-transition from a ferromagnetic to homogeneous phase, and we numerically confirm with large scale simulations the existence of a critical exponent associated to the largest Lyapunov exponent, although at variance with the theoretical estimate. The existence of chaos in the magnetized state evidenced by a positive Lyapunov exponent, even in the thermodynamic limit, is explained by the resonant coupling of individual particle oscillations to the diffusive motion of the center of mass of the system due to the thermal excitation of a classical Goldstone mode. The transition from "weak" to "strong" chaos occurs at the onset of the diffusive motion of the center of mass of the non-homogeneous equilibrium state, as expected. We also discuss thoroughly for the model the validity and limits of a geometrical approach for their analytical estimate.

* marciano@fis.unb.br

I. INTRODUCTION

Many body systems with long range interactions are known to have several properties that set them apart from more "usual" systems with short range interactions, such as ensemble inequivalence, negative heat capacity (with no second law violation), anomalous diffusion and non-Gaussian (quasi-) stationary states [1]. An interparticle interaction potential is said to be long ranged if it decays at large distances as $r^{-\alpha}$ with $\alpha \leq d$, d the spatial dimension, with a consequence that the total potential energy increasing superlinearly with volume [2, 3]. Some important physical system with long range interactions are non-neutral plasmas [4], self-gravitating systems [5], vortices in two-dimensional turbulent hydrodynamics [6] and free electron laser [7]. Simplified models were also largely considered in the literature and allowed a better understanding of the statistical mechanics of equilibrium and non-equilibrium of systems with long range interactions, such as one and two-dimensional self-gravitating systems [8, 9], the Hamiltonian Mean Field (HMF) and self-gravitating ring models [10, 11].

Much progress in the understanding of the relaxation properties in many-particle systems with long range forces came from numerical simulations of model systems [12–20]. Although the scaling of the relaxation time to equilibrium with N depends on the type of system and spatial dimension [21, 22], as a common feature it diverges with N, and as a consequences it never attains thermodynamic equilibrium for $N \to \infty$. In many cases this relaxation time is sufficiently large that even for finite N it can be considered infinite for practical purposes. If the equilibrium is reached, then its properties can be studied using the usual techniques of equilibrium statistical mechanics [1–3, 23].

Simplified models have been important in the study of the intricate interplay between chaotic dynamics, ergodic properties and statistical mechanics of systems with long range interactions, while Lyapunov exponents has proven to be a useful tool in the study of chaos in dynamical systems [24] and particularly also for long range systems [25–27]. The precise determination of Lypaunov exponents is an intricate task and usually requires a great numerical effort with very long integration times, that can become prohibitive for a system with a very large number of particles. A prescription for their analytic estimation is therefore of great relevance. Casetti, Pettini and collaborators developed an analytic method to obtain the scaling behavior of the Largest Lyapunov Exponent (LLE) [28, 29], and applied

to the HMF model by Firpo in Ref. [30].

The HMF model has been widely studied in the literature as a prototype for observations of some dynamical features of long range interacting systems [1]. It consists of N classical particles moving on a unit circle and globally coupled with Hamiltonian [10]:

$$H = \sum_{i=1}^{N} \frac{p_i^2}{2m} + \frac{1}{2N} \sum_{i,j=1}^{N} \left[1 - \cos\left(\theta_i - \theta_j\right)\right], \tag{1}$$

where θ_i and p_i are the position angle on the circle and p_i its conjugate momentum. The $1/N$ factor in the potential energy is the Kac factor introduced such that the total energy is extensive, and can be obtained from a change in the time unit. We can define by analogy the total magnetization and its components by:

$$\mathbf{M} = (M_x, M_y) = \frac{1}{N} \sum_{i=1}^{N} (\cos\theta_i, \sin\theta_i). \tag{2}$$

This system is exactly solvable and its equilibrium distribution function is given by [10]:

$$f_{\mathrm{eq}}(p, \theta) = \frac{\sqrt{\beta}}{(2\pi)^{3/2}\, \mathrm{I}_0(\beta)} e^{-\beta\left(p^2/2 - M\cos(\theta)\right)}, \tag{3}$$

where I_k is the Bessel function of the first kind with index k, and the origin for angles is chosen such that $M_y = 0$ and $M_x = M$. For a given inverse temperature β, the magnetization is obtained from the equation:

$$M = \frac{\mathrm{I}_1(\beta M)}{\mathrm{I}_0(\beta M)}, \tag{4}$$

with $M \equiv ||\mathbf{M}||$. The dependence of M on temperature is thus obtained by solving Eq. (4). A second order phase transition occurs at the critical energy per particle $e_c = E_c/N = 3/4$ and $T = 1/\beta = 0.5$ from a lower energy ferromagnetic phase to a higher energy phase with zero magnetization. Canonical or microcanonical ensembles are fully equivalent for the HMF model. Out of equilibrium phase transitions for this model were studied in some detail in [31].

In the present work we investigate the scaling with N of the LLE for the HMF model for larger values of N than in previous similar studies. We took special care to balance numerical accuracy and computing time optimization by comparing the tangent map and cloned dynamics methods (see below). This allowed us to refine and go beyond previous findings. Particularly we confirmed the existence of a new critical exponent corresponding

for the LLE theoretically predicted in [30], although with a different value of the critical exponent.

This paper is structured as follows: in section II we briefly recall the theory of Lyapunov Exponents and the numerical determination of the LLE. In section III we present and discuss our results for the HMF model and we close in section IV with some concluding remarks.

II. LYAPUNOV EXPONENTS

A Lyapunov Exponent (LE) quantify how the dynamics of the system is sensible to small differences in the initial conditions. With this aim, let us define the vector formed by coordinates in a n-dimensional phase space:

$$\mathbf{x} \equiv (\mathbf{x_1}, \mathbf{x_2}, ...\mathbf{x_n}). \tag{5}$$

which we suppose satisfy a set of n autonomous first-order differential equations:

$$\frac{d\mathbf{x}(\mathbf{t})}{dt} = F(\mathbf{x}(\mathbf{t})). \tag{6}$$

Equation (6) generates a flows in the phase space, and $F(\mathbf{x}(\mathbf{t}))$ is the velocity field of the flow. In order to measure contraction or stretching in the neighborhood of $\mathbf{x}(\mathbf{t})$, we consider two different solutions of Eq. (6) $\mathbf{x^{(1)}}(\mathbf{t})$ and $\mathbf{x^{(2)}}(\mathbf{t})$ and the difference vector $\mathbf{w} \equiv \mathbf{x}^{(2)}(t) - \mathbf{x}^{(1)}(t)$:

$$\mathbf{w} = (\delta x_1, \delta x_2, \ldots, \delta x_n). \tag{7}$$

The evolution equation for $\mathbf{w}$ is then:

$$\frac{d\mathbf{w}}{dt} = \mathbf{J}(\mathbf{x}(t))\mathbf{w}, \tag{8}$$

with $\mathbf{J}$ the $N \times N$ Jacobian matrix of the flow. Assuming that the elements of $\mathbf{J}$ are continuous bounded functions of t for $t \to \infty$, then the solutions of (8) grow no faster than $\exp(\lambda t)$, for some constant λ.

The Lyapunov Exponent for a given initial condition $\mathbf{w}(0)$ is defined by

$$\lambda \equiv \lim_{t\to\infty} \frac{1}{t} \ln\left(\frac{||\mathbf{w}(t)||}{||\mathbf{w}(0)||}\right). \tag{9}$$

In a n-dimensional problem we have n Lyapunov exponents, each one referring to the divergence degree of specific directions of the system. All of them form a set called Lyapunov Spectrum (LS), which usually are organized as:

$$\lambda_1 \geq \lambda_2 \geq \cdots \geq \lambda_N. \tag{10}$$

If the LLE λ_1 is positive then neighbor trajectories tend to diverge exponentially which implies a chaotic regime. Due to the Liouville theorem, the Lyapunov spectrum of a Hamiltonian system is, as those considered below, satisfies the relation (Pesin's theorem):

$$\lambda_i = -\lambda_{2N-i+1}. \tag{11}$$

Another important result relates the Kolmogorov-Sinai entropy and the Lyapunov spectrum. The former measures exponential rate of information production in a dynamical system [24] and according to Pesin's theorem can be obtained as the sum of all positive Lyapunov exponents [32]. We now briefly present two approaches [33, 34] for the numerical determination of the Lyapunov exponents.

A. Numeric determination of the LLE

In the tangent map method, Eq. (7) is solved for short times by replacing $\mathbf{x}(t)$ by $\mathbf{x}^* = \mathbf{x}(t^*)$, where t^* stands for the initial condition at each step of the algorithm:

$$\frac{d\mathbf{w}}{dt} = \mathbf{J}|_{x=x^*}\mathbf{w}, \tag{12}$$

One then solves the original nonlinear system in Eq. (6) and the linearized equations (12). The steps for determining the Lyapunov exponent are:

1. For the nonlinear system (6) impose an initial condition $\mathbf{x}_0$, and an initial condition $\mathbf{w}_0 = \boldsymbol{\delta}_0$ for the linearized equations, with $||\boldsymbol{\delta}|| = \epsilon$ and $\epsilon \ll 1$.

2. Both differential equations are integrated for a time interval T. This results in $\mathbf{x}_0 \to \mathbf{x}(T)$ and $\boldsymbol{\delta}_0 \to \boldsymbol{\delta}_1 \equiv \mathbf{w}(T)$;

3. After each integration interval T, normalize the correspoding difference vector $\boldsymbol{\delta}_k$ to ϵ and use the resulting vector as a new initial condition for solving the linearized equations;

4. The LLE is obtained from the average:

$$\lambda_1 = \frac{1}{KT}\sum_{k=1}^{K} \ln \frac{||\boldsymbol{\delta}_k||}{\epsilon}, \tag{13}$$

where K is chose in order to achieve convergence in the value of λ_1.

In the cloned dynamics method [33], one defines a reference trajectory and a perturbed trajectory (cloned trajectory) obtained by perturbing the initial condition of the reference trajectory. Both trajectories are then obtained by solving the full nonlinear system (6). The remaining steps are the same as for the tangent map method. Denoting $\mathbf{x}_0$ as the initial conditions for the reference system, and $\mathbf{x}_0 + \boldsymbol{\delta}_i$ the initial conditions for the clone orbits, with $||\boldsymbol{\delta}_i|| = \epsilon$. The remaining steps are essentially the same as for the tangent map method.

Both methods have similar convergence properties [36], and for the purposes of the present work the computations will require large values of N. As a consequence, a parallel implementation becomes highly useful. The cloned dynamics method is more suited for the reasons that we discuss now. The equations of motion for the HMF model derived from the Hamiltonian in Eq. (1) are:

$$\begin{aligned} \dot{\theta}_i &= p_i, \\ \dot{p}_i &= F_i = -\frac{1}{N}\sum_{j=1}^{N} \sin\left(\theta_i - \theta_j\right) = -\sin\theta_i \, M_x + \cos\theta_i \, M_y, \end{aligned} \tag{14}$$

with F_i the generalized force acting on particle i. As a consequence, we must calculate the values of magnetization components M_x and M_y, with a numerical effort proportional to N, and them compute with these results the N components of the force, with an overall numerical effort proportional to N. Let us now consider the numerical effort to solve the linearized equations of motion for the HMF model around a point in phase space (θ_i^*, p_i^*). By writing $\theta_i(t) = \theta_i^* + \delta\theta_i(t)$ and $p_i(t) = p_i^* + \delta p_i(t)$, these equations are given by:

$$\delta\dot{\theta}_i = p_i^* + \delta p_i, \tag{15}$$

$$\begin{aligned} \delta\dot{p}_i = &-\sin\theta_i^* \, M_x^* + \cos\theta_i^* \, M_y^* - \delta\theta_i \left[\cos\theta_i^* \, M_x^* + \sin\theta_i^* \, M_x^*\right] \\ &+\frac{1}{N}\sum_{j=1}^{N} \cos\left(\theta_i^* - \theta_j^*\right) \delta\theta_j, \end{aligned} \tag{16}$$

where the components of the magnetization are computed at the angles θ_i^* and are denoted M_x^* and M_y^*. The first and second terms in the right-hand side of Eq. (16) result in a numeric effort proportional to N, while the last term this effort is proportional to N^2, as we have to compute N terms, each one involving N computations. This same term must be computed after each time step as it depends on time through $\delta\theta_j$. Since both methods have similar convergence properties, and the cloned dynamics being the more effective numerically, it will be used in all computations in the present paper. We implemented the algorithm using the

C language extension CUDA [37] for parallel programming in Graphics Processing Units (GPUs) and a fourth-order symplectic integrator [38]. The speed-up gain over a serial implementation is of the order of 50 to 100 times [39].

B. An analytic estimate for the LLE

The LLE for the HMF model was investigated numerically by Yamaguchi [40], and then latter estimated by Latora, Rapisarda and Ruffo [41] from a random matrix approach of Parisi and Vulpiani [42], and by Firpo [30] using the differential geometry approach by Pettini and collaborators [43–45]. In the latter approach, the dynamics of the N particle system is reformulated in the framework of Riemannian geometry, where the trajectories correspond to geodesics of an underlying metric. Chaos then comes from the instability of the geodesic flow, that at its turn depends on the properties of the curvature of the Riemannian manifold. Chaos can also result from a parametric instability of the fluctuation of the curvature along the system trajectory as represented in the manifold.

In order for the present paper to be self contained, we succinctly present here the the main results of the geometrical approach to the computation of Lyapunov exponents and chaos from Refs. [29] and [43] (where the reader can find more details). We consider a system of N identical particles with unit mass and Hamiltonian:

$$H = \sum_{i=1}^{N} \frac{p_i^2}{2} + V(\mathbf{r}_1, \ldots, \mathbf{r}_N), \tag{17}$$

where $\mathbf{r}_i$ is the position vector of particle i, $\mathbf{p}_i$ its canonically conjugate momentum and V the potential energy. Considering two solutions $\overline{\mathbf{r}}_i(t)$ and $\mathbf{r}_i(t)$, $i = 1, \ldots, N$, initially close to one another: $\overline{\mathbf{r}}_i(t) = \mathbf{r}_i(t) + \boldsymbol{\xi}_i(t)$. The linearized equations of motion for the small variations $\xi_1(t)$ are given by:

$$\frac{d^2\boldsymbol{\xi}_i(t)}{dt^2} + \sum_{j=1}^{N} \frac{\partial^2 V}{\partial \mathbf{r}_i \partial \mathbf{r}_j} \cdot \boldsymbol{\xi}_j(t) = 0. \tag{18}$$

The maximal Lyapunov exponent is then obtained from:

$$\lambda = \lim_{t\to\infty} \frac{1}{2t} \ln \left(\frac{||\boldsymbol{\xi}(t)||^2}{||\boldsymbol{\xi}(0)||} \right), \tag{19}$$

where

$$||\boldsymbol{\xi}(t)|| \equiv \sqrt{\boldsymbol{\xi}_1(t)^2 + \cdots + \boldsymbol{\xi}_N(t)}. \tag{20}$$

Each component $\boldsymbol{\xi}_i$ satisfies the single same equation:

$$\frac{d^2\psi(t)}{dt^2} + k(t)\psi(t), \tag{21}$$

where $k(t)$ is a stochastic process describing the time evolution of the curvature along a trajectory in phase space. Since the solutions of Eq. (21) are given in term of the averages $\langle \cdots \rangle$ over many realizations of the stochastic process, Eq. (19) assumes the form:

$$\lambda = \lim_{t\to\infty} \frac{1}{t} \frac{\langle \psi(t) \rangle}{\langle \psi(0) \rangle}. \tag{22}$$

The solution for the average is obtained from a perturbative expansion in the amplitude of the fluctuations of the stochastic process, which are small for large N. By introducing a smallness multiplicative parameter in the stochastic process as $k(t) \to \alpha k(t)$, where $\alpha \ll 1$, an supposing that fluctuations are delta correlated, a perturbative solution of Eq. (21) in powers of α can be obtained [29, 46]. In the case that $k(t)$ is a Gaussian process, this solution becomes exact.

An estimate of the LLE λ_1, with the extra assumption that the curvature along a trajectory is well represented by a Gaussian process, was obtained in Ref. [43], with very good agreement with numerical results for the Fermi-Pasta-Ulam model and the 1D XY model [45]. The LLE is given in then given by [43]:

$$\lambda_1 = \frac{\Lambda}{2} - \frac{2\kappa_0}{3\Lambda}, \tag{23}$$

where

$$\Lambda = \left(2\sigma_k^2 \tau + \sqrt{\frac{64}{27}\kappa_0^3 + 4\sigma_k^4 \tau^2} \right)^{1/3}, \tag{24}$$

$$\tau = \frac{\pi\sqrt{\kappa_0}}{2\sqrt{\kappa_0}\sqrt{\kappa_0 + \sigma_k} + \pi\sigma_k}, \tag{25}$$

with κ_0 and σ_k^2 the average curvature and the fluctuations around its mean value, respectively, τ being a characteristic time for the stochastic process. For the HMF model, Firpo obtained a closed form expression for the quantities κ_0 and σ_k [30], such that the (Ricci) scalar curvature in the Riemannian manifold is given by $\kappa_R = M^2$. The next step consists to take $\kappa_0 = \langle M^2 \rangle_\mu$, i. e. the microcanonical average of M^2. The variance of the curvature fluctuations in the microcanonical ensemble was obtained in [30] as:

$$\sigma_k^2 = \langle \delta^2 k_R \rangle_c \left(1 + \frac{\beta^2}{2} \langle \delta^2 k_R \rangle_c \right)^{-1}, \tag{26}$$

where $\langle \delta^2 k_R \rangle_c$ is the variance of the fluctuations in the canonical ensemble:

$$\langle \delta^2 k_R \rangle_c = 4M \frac{\partial M}{\partial \beta}, \tag{27}$$

with M given by the solution of Eq. (3). It is worth noting that even if $k(t)$ is not Gaussian, the expressions above remain valid up to first order in α.

Previous results showed that in the non-magnetized phase the Lyapunov exponent tends to zero as N increases, with a scaling with $N^{-1/3}$ observed numerical in Ref. [41] and explained theoretically in [30]. In the ferromagnetic phase, a more complicate picture emerges. Manos and Ruffo observed numerically a transition from a weak to a strong chaoticity regimes at low energy [47], and related it to the time dependence of the phase of the magnetization vector, which becomes strongly time dependent around the same energy. A critical exponent for the LLE was predicted by Firpo [30] in the vicinity of the second order phase transition for $e < e_c$ in the form

$$\lambda_1 \propto (e_c - e)^{\xi}, \tag{28}$$

with an exponent $\xi = 1/6$. Ginelli and collaborators obtained a different value $\xi = 1/2$ from numerical results, the same critical behavior as the magnetization [48].

III. RESULTS

The first point to consider is whether the fluctuations of the curvature, i. e. of M^2 for the HMF model, can be modeled by an uncorrelated Gaussian process, as considered in Refs [30, 43]. Figure 1 show the distributions of the fluctuations of the curvature $\kappa_R = M^2$ for a few values of energy, and the correlation function for the fluctuations $\langle M(t_0 - \tau)^2 M(t_0)^2 \rangle - \langle M^2 \rangle^2$ for a few energy values. In the ferromagnetic state the fluctuations well represented by a Gaussian distribution, but the correlation time, i. e. the time for correlations to be negligible, can be very large. The correlation time is small only at higher energies. In the homogeneous phase, correlations of the fluctuations of the curvature are also non-negligible, and their distribution is non-Gaussian quite close to an exponential function. In fact it is more natural to expect that the fluctuations of the magnetization components are Gaussian rather than those of M^2. One can show that the distributions in Fig. 1 for the magnetized states are those obtained from a Gaussian distribution in the change of variables $M_x \to M_x^2$ (supposing $M_y = 0$) and a small standard deviation relative

to the average. The distributions for the values of M are given in Fig. 2. Below the critical energy the distribution is Gaussian, while above the phase transition it is well described by a function of the form $bM\exp(-aM^2)$, with a and b constants. In obtaining Eqs. (23–25) the central assumption was that fluctuations are delta correlated. This is clearly valid only for higher energies, where as shown below the predicted $N^{-1/3}$ scaling of the LLE is observed. Deviations from the theoretical predictions are thus expected for lower energies due to strong correlations in the fluctuations of the curvature.

Figure 3 shows the plot of the LLE λ_1 as a function of energy for some values of N, alongside the theoretical prediction of Ref. [30]. In the ferromagnetic phase the theoretical results agree only qualitatively with numerical results, predicting a maximum of the LLE for an energy below the critical energy e_c, but not its position, and also that λ_1 goes to zero at the phase transition. The left panel in Fig. 4 shows a reasonable data collapse if the exponent are rescaled by $N^{-1/3}$, that nevertheless becomes not so good for energies closer to the phase transition as seen on the left panel of Fig. 4. Figure 5 shows λ_1 as a function of N for some energy energy values in the non-magnetized state. The predicted $N^{-1/3}$ scale is observed far from the phase transition. This is true up to quite higher values of N. Figure 6 shows the results for λ_1 for the energy $e = 0.8$ for $N = 1000$ up to $N = 5\,000\,000$ with scaling very close to $N^{1/4}$. Figure 7 shows similar results for the larger values of N, much larger than in previous studies, with a scaling of $N^{-0.3}$, in approximate agreement with the theoretical result. This seems to indicate that, as expected, the theoretical results apply for sufficiently large values of N. How large it must be is of course model dependent. In the present case this implies N at least of the order 10^6. Figure 8 shows the correlation function of the fluctuations of the Riemannian curvature. Such fluctuations are not delta correlated close to the phase transition and thus explaining the theoretical scaling is easily observed at higher energies. It is also important to note that for non-Gaussian fluctuations the solution of Eq. (21) is only valid at order α^2, and therefore is more accurate for smaller α and equivalently greater N.

For the ferromagnetic phase, Figure 9 shows the LLE λ_1 as a function of N for a few energy values. A plateau is visible for each of the energy values indicating that λ_1 has a limit value for $N \to \infty$. As a consequence, no power law scaling of the form N^ν is possible. Manos and Ruffo studying the same system observed a transition from weak to strong chaos at an energy $e_w \approx 0.15$, such that below e_w the LLE is much smaller and scales as $N^{-1/3}$ [47].

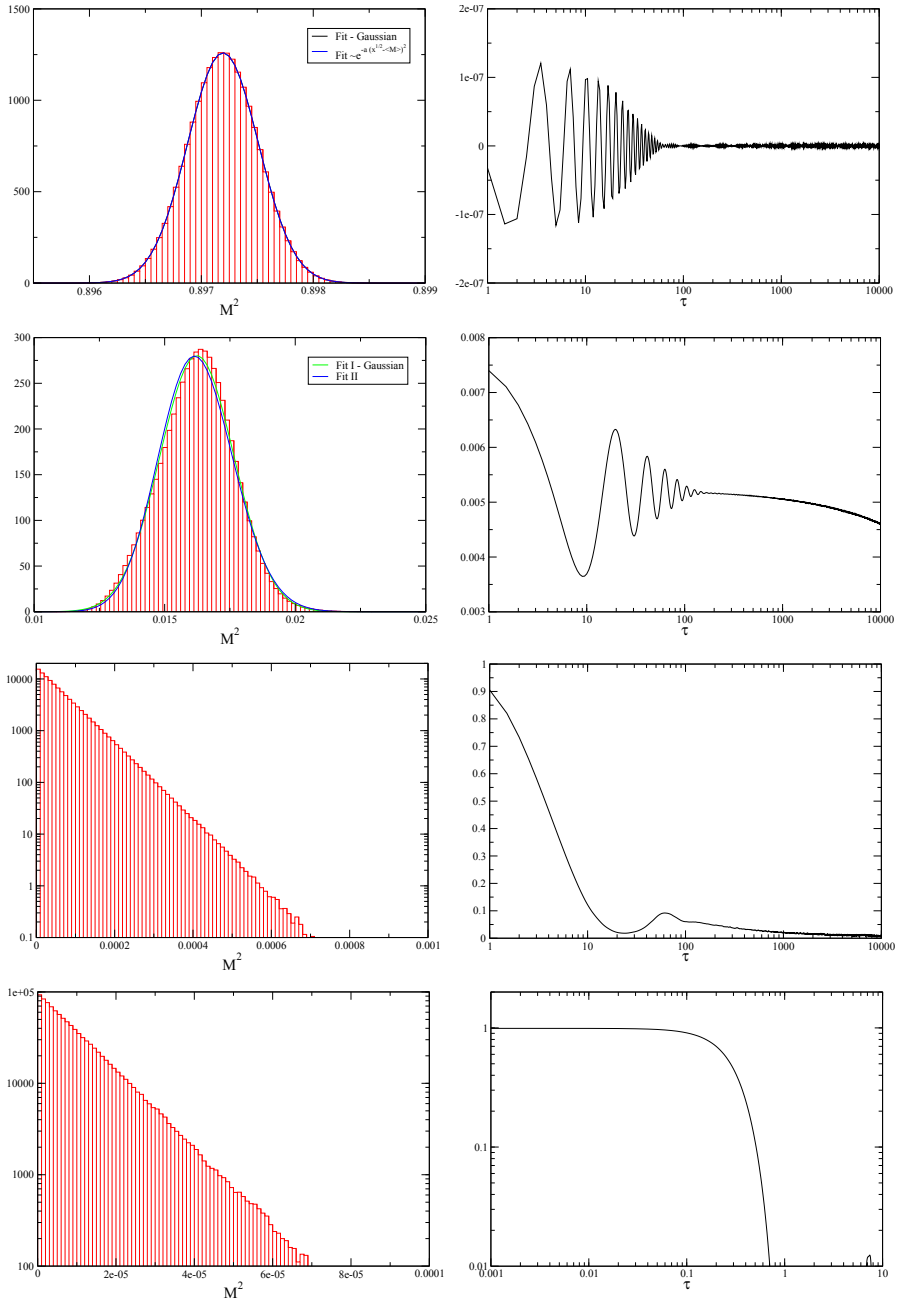

FIG. 1. (Color online) a) Distribution (histogram) of fluctuations of the curvature $\kappa_R = M^2$ for the equilibrium state with energy per particle $e = 0.1$, $N = 100\,000$, integration time step $\Delta t = 0.05$ and total integration time $t_f = 10^5$. The continuous line is a least squares fit with a Gaussian distribution. b) Correlation $\langle M(t_0 - \tau)M(t_0)\rangle - \langle M\rangle^2$ as a function of τ. c) and d) Same as (a) and (b) for e=0.74. e) Log plot of the distribution of fluctuations of κ_R for $e = 0.8$ where an exponential distribution is clearly visible. f) Correlations for $e = 0.8$. g) same as (a) with $e = 5.0$. g) Same as (b) for $e = 5.0$ In all cases the total simulation time is $t_f = 10^7$, integration time step $\Delta t = 0.5$, except (g) and (h) where $t_f = 10^4$ and $\Delta t = 10^{-2}$.

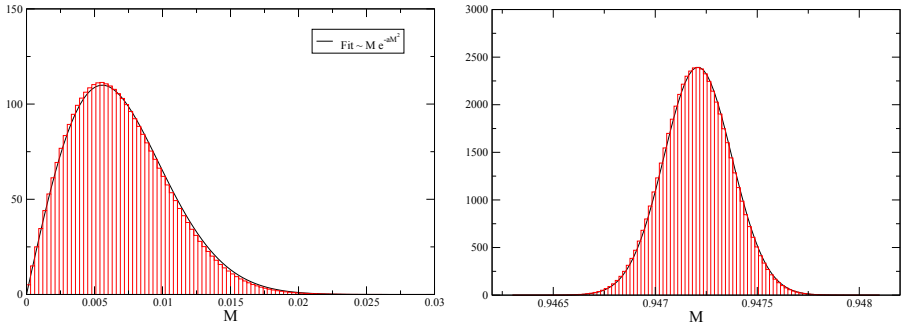

FIG. 2. (Color online) Left Panel: Distribution of values of the magnetization M for the equilibrium state with $e = 0.8$. The continuous line is a least squares fit of the expression $bM \exp\left(-aM^2\right)$, with a and b constants. Right Panel: Same as in the left panel but for $e = 0.1$. The continuous line is a fitting of a Gaussian function $a \exp\left(-a(M - \langle M \rangle)^2\right)$.

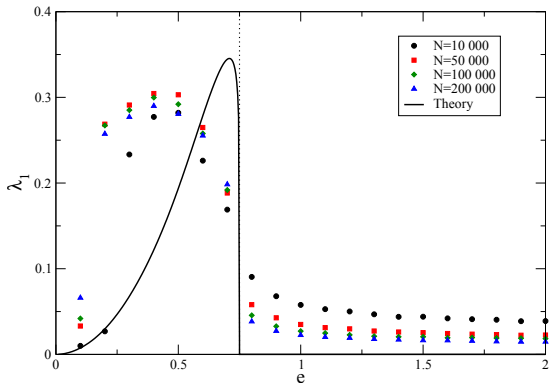

FIG. 3. (Color online) Largest Lyapunov exponent λ_1 as a function of energy per particle e for a few values of N. The continuous line is the theoretical result from Ref. [26], and the vertical dotted line indicates the position of the second order phase transition. The parameters used in the simulation where an interaction time step $\Delta t = 0.05$, $T = 10.0$ and total simulation time $t_f = 2 \times 10^5$.

This is at variance with the results in Fig. 9 and requires an explanation. The same authors using the generalized alignment indices method [49] showed that at this energy the fraction of chaotic orbits of the system increases rapidly from a very low (less than 1%) to a very large value (close to 100%). As a consequence, correctly measuring the LLE proves to be a difficult task as the probability that of a given randomly chosen orbit and another nearby orbit (the cloned orbit) to be non-chaotic are high, which at its turn implies that in most

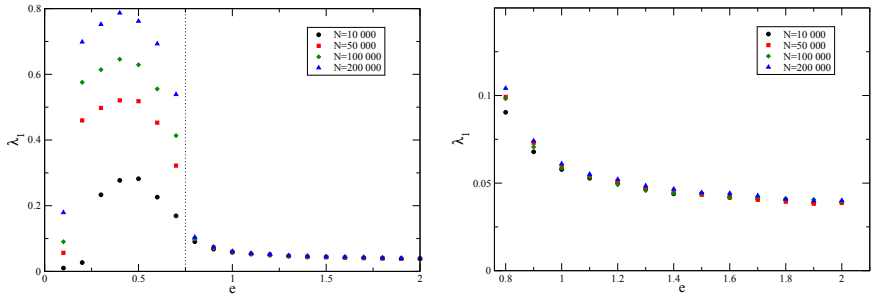

FIG. 4. (Color online) Left panel: same as in the left panel of Fig. 3 but with λ_1 rescaled by $(N/10\,000)^{-1/3}$. Right panel: zoom over the energy range $(0.75, 2.0)$.

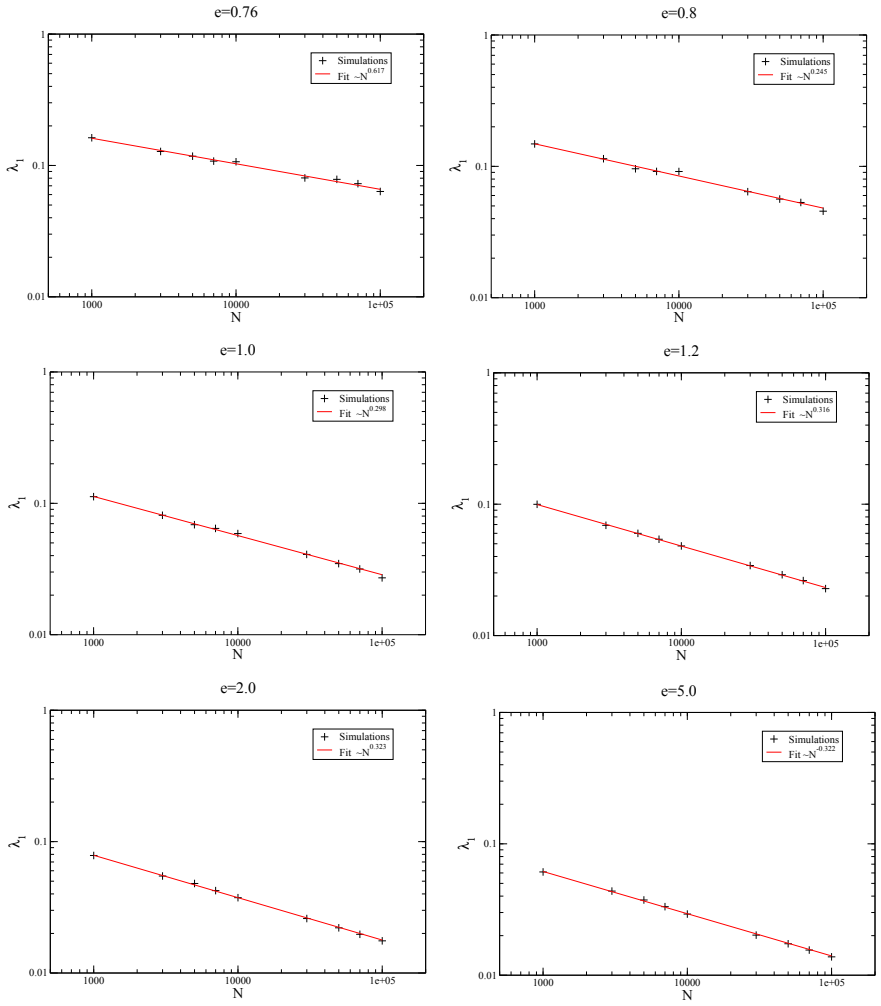

FIG. 5. (Color online) Largest Lyapunov exponent λ_1 for a few energy values $e = 0.76$, 0.8, 1.0, 1.2, 2.0 and 5.0. The continuous line is a least squares fit of a power law in N.

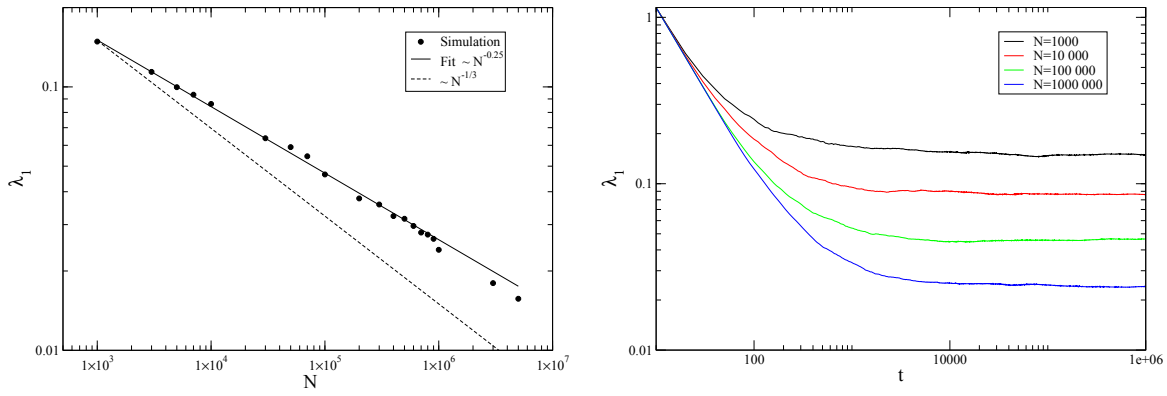

FIG. 6. (Color online) Left panel: Largest Lyapunov exponent λ_1 for $e = 0.8$ and values of N ranging from $N = 1000$ up to $N = 50\,000\,000$ from the cloned dynamics method, and a least squares fit of N^β with $\beta \approx 0.25$. A curve proportional to $N^{-1/3}$ (dashed line) is also shown for comparison purposes. Right panel: values of λ_1 computed from Eq. (13) as a function of simulation time $t = nT$ showing that the results in the graphic on the left panel are fully converged.

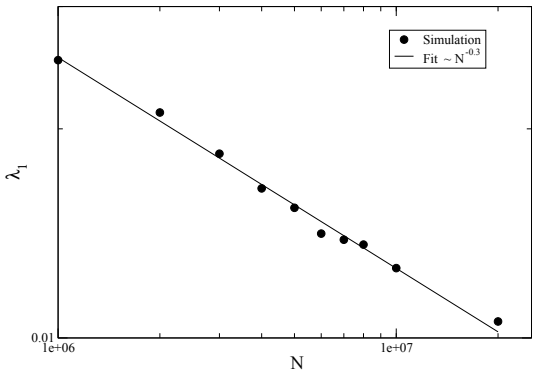

FIG. 7. Largest Lyapunov exponent λ_1 for N from $N = 1000\,000$ up to $N = 20\,000\,000$ (circles) and a least squares fit of a power law N^β with $\beta \approx 0.3$, close to the predicted $N^{1/3}$ scaling.

cases the resulting value of λ_1 will be much smaller than the actual value. In order to illustrate this point, we show in Fig. 10 the convergence of the LLE λ_1 for 10 different realizations of the same equilibrium state for $e = 0.1$. We see that for $N = 5000$, 80% of the obtained values for λ_1 are much smaller than the actual value, corresponding to the highest obtained value in the set of simulations, while for $N = 10000$ this fraction is smaller, although the convergence is much slower depending on the realization. In fact the fraction of chaotic orbits increases with N [47] and thus the fraction of realizations that converge to

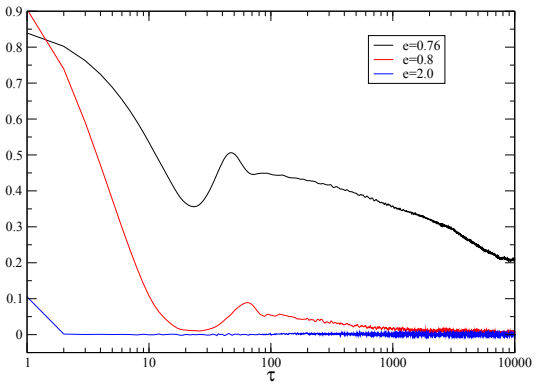

FIG. 8. Correlation function $\langle M(t_0+\tau)^2 M(t_0)^2\rangle$ for the fluctuations in the curvature $\kappa_R = M^2$ for a few values of e and $N = 100\,000$.

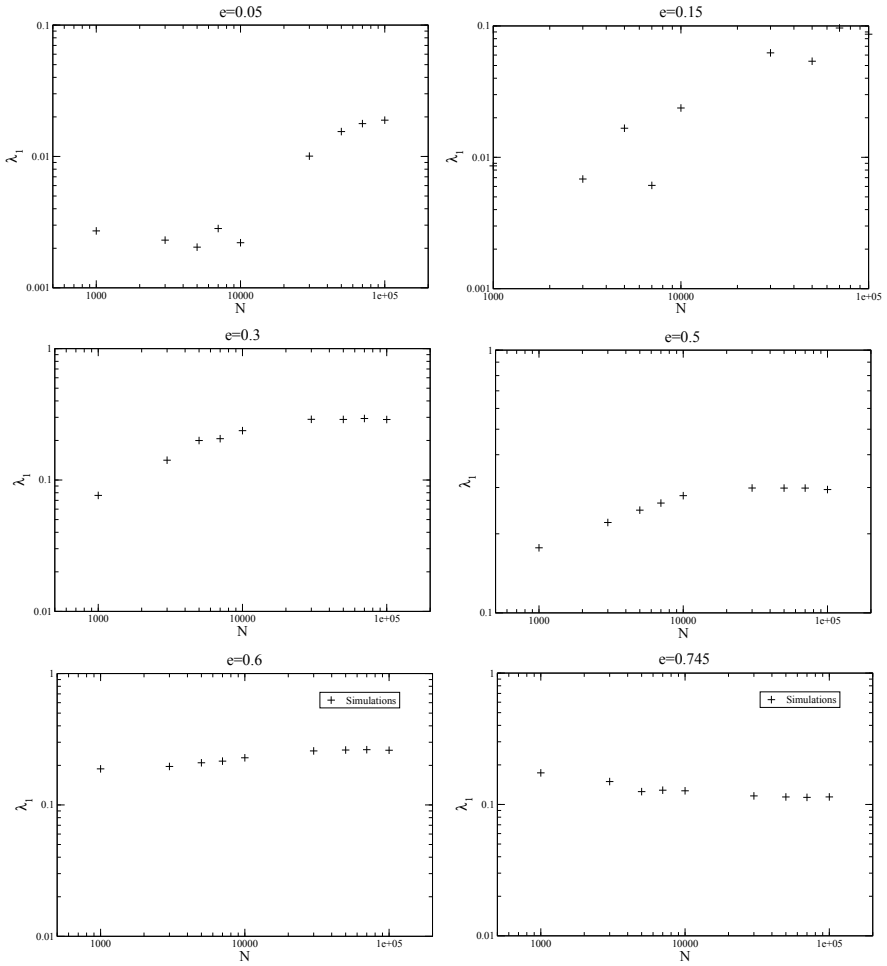

FIG. 9. Largest Lyapunov exponent λ_1 for a few energy values $e = 0.05$, 0.15, 0.3, 0.5, 0.6 and 0.745.

the correct value of λ_1 increases also with N. Thus in this case, when the fraction of chaotic orbits is very small, many realizations are needed in order to correctly determine the LLE from the highest value. The result for $e = 0.1$ for some values of N is shown in Fig. 11.

The LLE as a function of energy in the ferromagnetic phase for $N = 100\,000$ is show in

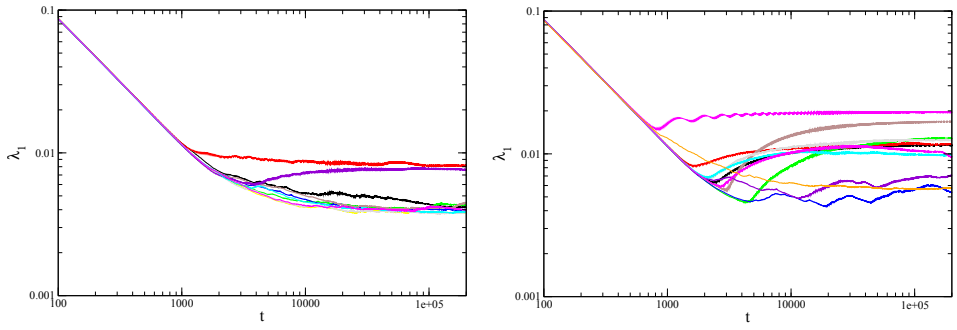

FIG. 10. Left Panel: Largest Lyapunov exponent λ_1 as a function of time using the cloned dynamics method, for $e = 0.1$ and $N = 5000$ for 10 different realizations. Right Panel: same as the left panel but with $N = 10\,000$.

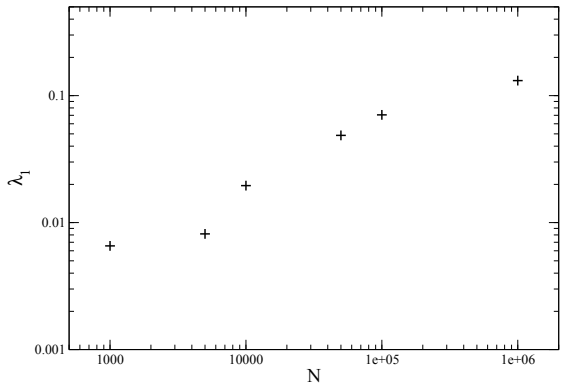

FIG. 11. Largest Lyapunov exponent λ_1 from the largest value obtained from the cloned dynamics from 10 realizations of the equilibrium state for $e = 0.1$ as a function of N.

Fig. 12. The transition from weak to strong chaos can be explained from the equilibrium properties of the system. The equilibrium spatial distribution obtained by integrating f_{eq} in Eq. (3) over the momentum, is given by

$$\rho_{eq}(\theta) = C_N \exp\left(\beta M \cos(\theta)\right), \tag{29}$$

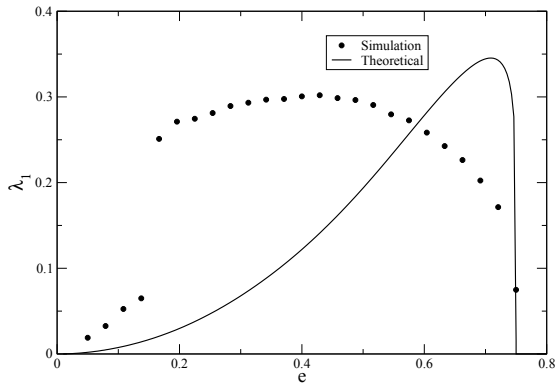

FIG. 12. Largest Lyapunov exponent λ_1 as a function of energy for $N = 100\,000$ for $e < e_c = 0.75$ from numerical simulations. The transition from weak to strong chaoticity is clearly visible at $e \approx 0.15$. The continuous line is the theoretical prediction.

with C_N a normalization constant. In Eq. (29) the maximum of $\rho_{eq}(\theta)$ occurs at $\theta = 0$ by a choice of the origin for the angles. The values of the spatial distribution at $\theta = \pi$ as a function of energy are shown in Fig. 13. The transition from weak to strong chaos occurs

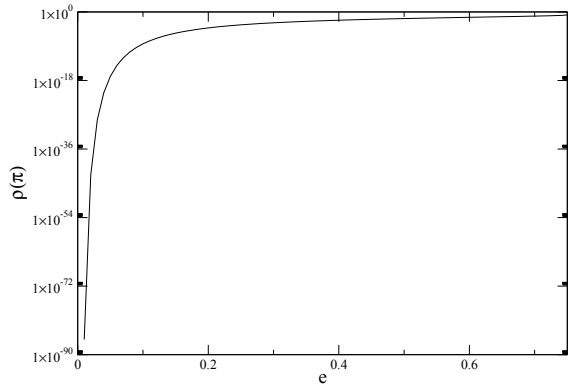

FIG. 13. Value of the spatial distribution function $\rho_{eq}(\theta)$ in Eq. (29) at $\theta = \pi$.

at the energy value e_w when $\rho_{eq}(\pi)$ attains a significant value and particles start to cross at the border $\theta = \pi$. This induces the excitation of a classical Goldstone mode resulting in an effective diffusive motion of the equilibrium state around the circle [50], and consequently oscillation of the magnetization vector, which is coupled to the individual motions of the particles in Eq. (14). A parametric resonance then triggers the chaotic behavior. For $e < e_w$ these oscillations are almost absent and the system weakly chaotic with only a small fraction of the orbits being chaotic.

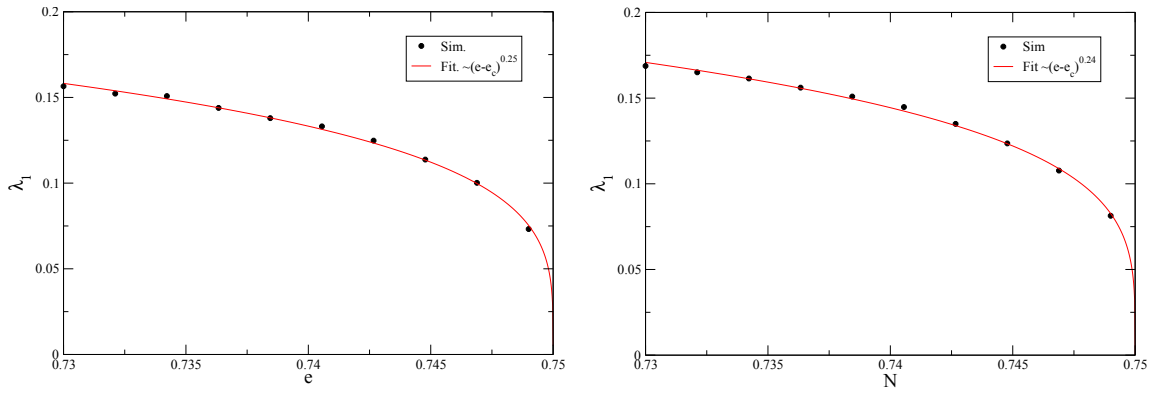

FIG. 14. Largest Lyapunov exponent λ_1 as a function of energy close to the phase transition for $N = 100\,000$ (left panel) and $N = 1000\,000$ (right panel). The value on λ_1 has already converged to a plateau (see Fig. 9). The continuous line is a least squares fit with a critical exponent ≈ 0.25 ($N = 100\,000$) and ≈ 0.24 ($N = 1000\,000$). The simulation parameters are $T = 10.0$, $t_f = 2 \times 10^5$,i $\Delta t = 0.05$ and $\epsilon = 10^{-3}$.

In order to investigate the possible critical behavior of the LLE for energies close to e_c from below as in Eq. (28), we computed λ_1 at high precision ensuring the convergence or the cloned dynamics method. The results are shown in Fig. 14 for $N = 100000$ and $N = 1000000$ and some energy values. The fitting of Eq. (28) is very good for both values of N, with an exponent close to $\xi \approx 1/4$ instead of the theoretical value $1/6$. This is possibly due to important correlations in the fluctuations of $\kappa_R = M^2$, which become more important close to the phase transition, as discussed above. The difference with respect to the exponent $\xi \approx 1/2$ obtained in Ref. [48] can be explained by our longer simulation time and higher values of N which were made feasibly by a massively parallel implementation of our numeric code.

IV. CONCLUDING REMARKS

This paper addressed the study of chaoticity in the HMF model from the determination of LLE. This paradigmatic model has been widely used in the literature to understand the behavior and some properties of long range interacting systems. For reasons of computational efficiency we used the cloned dynamics method to compute the LLE (a more through comparison of methods can be found in [36]). Our numerical implementation CUDA allowed

to investigate the LLE for a wide range of energies, and values of N as large as 2×10^7. The size of the system has been essential to describe the main characteristics features of the exponents. For the homogeneous phase ($e \geq 0.75$,) at all energies, it was shown clearly that the exponents scales with the system size as N^β with β approaching $-1/3$, the theoretical predicted value, with increasing N or increasing energy. This comes from non negligible self-correlations in time of the fluctuations of the scalar curvature used in the geometric approach for the theoretical determination of the LLE. For energies below the transition energy we could not find any scale with the system size.

We confirmed numerically the existence of a critical exponent associated to the Lyapunov exponent as defined in Eq. (28). The value we have obtained for this exponent is $\xi \approx 1/4$ is at variance with the predicted theoretical value of $1/6$ and with the value of $1/2$ obtained in Ref. [48]. With respect to the former, this difference is explainable by the fact that the stochastic process representing the Riemannian curvature on the underlying manifold in not delta correlated, as shown in Fig. 1d. Our parallel implementation of the algorithm for computing the LLE allowed a significant improvement in the accuracy of the numerical results, which possibly explains the variance with the result in [48].

Whether such a critical exponent also occurs for other long range interacting systems is an open question that requires to be investigated. A similar but much computationally demanding study for the self-gravitating ring model [11] is the subject of ongoing work.

V. ACKNOWLEDGMENTS

MAA and TMRF would like to thank M.-C. Firpo for fruitful discussions. TMRF was partially financed by CNPq (Brazil) and LAMF was financed by CAPES (Brazil).

---

[1] A. Campa, T. Dauxois, D. Fanelli and S. Ruffo, *Physics of Long-Range Interacting Systems*,

[2] A. Campa, T. Dauxois, and S. Ruffo, Phys. Rep. **480** (2009) 57.

[3] T. Dauxois, S. Ruffo, E. Arimondo and M. Wilkens Eds, *Dynamics and Thermodynamics of Systems with Long-Range Interactions*, Springer (Berlin,2002).

[4] F. B. Rizzato, R. Pakter and Y. Levin, Phys. Rev. E **80**, 021109 (2009).

[5] T. Padmanabhan, Phys. Rep. **188**, 285 (1990).

[6] A. Venaille, T. Dauxois, and S. Ruffo, arXiv: 1503.07904.

[7] A. Antoniazzi, Y. Elskens, D. Fanelli and S. Ruffo, Eur. Phys. J. B **50**, 603 (2006).

[8] Lj. Milanović, H. A. Posch and W. Thirring, J. Stat. Phys. **124**, 843 (2006).

[9] T. N. Teles, Y. Levin, R. Pakter and F. B. Rizzato, J. Stat. Mech. P05007 (2010).

[10] M. Antoni and S. Ruffo, Phys. Rev. E **52**, 2361 (1995).

[11] Y. Sota, O. Igushi, M. Morikawa, T. Tatekawa and K. Maeda, Phys. Rev. E, **64** (2001) 056133.

[12] T. M. Rocha Filho, M. A. Amato, A. E. Santana, A. Figueiredo and and J. R. Steiner, Phys. Rev. E **89**, 032116 (2014).

[13] F. Baldovin and E. Orlandini, Phys. Rev. Lett. **97**, 100601 (2006).

[14] P.-H. Chavanis, Physica A **365**, 102 (2006).

[15] P. de Buyl, D. Fanelli, R. Bachelard and G. De Ninno, Phys. Rev. Sep. Top. Acc. Beams **12**, 060704 (2009).

[16] A. Gabrielli, M. Joyce and B. Marcos, Phys. Rev. Lett. **105**, 210602 (2010).

[17] S. Gupta and D. Mukamel, J. Stat. Mech P03015 (2011).

[18] M. Assllani, D. Fanelli, A. Turchi, T. Carletti and X. Leoncini, Phys. Rev. E **85**, 021148 (2012).

[19] R. Pakter and Y. Levin, Phys. Rev. Lett. **110**, 140601 (2013).

[20] R. Bachelard, C. Chandre, D. Fanelli, X. Leoncini and S. Ruffo, Phys. Rev. Lett. **101**, 260603 (2008).

[21] T. M. Rocha Filho, A. E. Santana, M. A. Amato and A. Figueiredo, Phys. Rev. E **90**, 032133 (2014).

[22] C. R. Lourenço and T. M. Rocha Filho, Phys. Rev. E **92**, 012117 (2015).

[23] Y. Levin, R. Pakter, F. B. Rizzato and T. N. Teles, Phys. Rep. **535**, 1 (2014).

[24] E. Ott, *Chaos in Dynamical Systems*, Cambridge Univ. Press (Cambrigde, 1993).

[25] R. O. Vallejos and C. Anteneodo, Physica A **340**, 178 (2004).

[26] M.-C. Firpo and S. Ruffo, J. Phys. A **34**, L511 (2001).

[27] C. Anteneodo and R. O. Vallejos, Phys. Rev. E **65**, 016210 (2001).

[28] M. Pettini, Phys. Rev. E **47**, 828 (1993).

[29] L. Casetti, M. Pettini and E. G. D. Cohen, Phys. Rep. **337**, 238 (2000).

[30] M.-C. Firpo, Phys. Rev. E **57**, 6599 (1998).

[31] T. M. Rocha Filho, M. A. Amato and A. Figueiredo, Phys. Rev. E **85**, 062103 (2012).

[32] J. P. Eckmann and D. Ruelle, Rev. Mod. Phys. **57**, 617 (1985).

[33] D. C. Soriano, F. I. Fazanaro, R. Suyama, J. R. Oliveira, R. Attux and M. K. Madrid, Nonlinear Dyn. **67**, 413 (2012).

[34] T. Laffargue, K-D. N. T. Lam, J. Kurchan and J. Tailleur, J. Phys. A **46**, 254002 (2013).

[35] J. Marão, X. Liu and A. Figueiredo, Chaos, Solitons & Fractals **45**, 1067 (2012).

[36] L. H. Miranda Filho, T. M. Rocha Filho, M. A. Amato and Y. Elskens, In preparation.

[37] NVIDIA, CUDA Programming Guide, Ver. 4.0, 2011.

[38] H. Yoshida, Phys. Lett. A **150** (1990) 262.

[39] T. M. Rocha Filho, Comp. Phys. Comm. **185**, 1364 (2014).

[40] Y. Y. Yamaguchi, Prog. Theor. Phys. **95**, 717 (1996).

[41] V. Latora, A. Rapisarda and S. Ruffo, Phys. Rev. Lett. **80**, 692 (1998).

[42] G. Parisi and A. Vulpiani, J. Phys. A **19**, L425 (1986).

[43] L. Casetti, R. Livi and M. Pettini, Phys. Rev. Lett. **74**, 375 (1995).

[44] L. Caiani, L. Casetti, C. Clementi and M. Pettini, Phys. Rev. Lett. **79**, 4361 (1997).

[45] L. Casetti, M. Pettini and E. G. D. Cohen, Phys. Rep. **337**, 237 (2000).

[46] N. G. Van Kampen, Phys. Rep. **24** (1976) 71.

[47] T. Manos, and S. Ruffo, Transp. Theory Stat. Phys. **40**, 360-381 (2011).

[48] F. Ginelli, K. A. Takeuchi, H. Chaté, A. Politi and A. Torcini, Phys. Rev. E **84**, 066211 (2011).

[49] C. Skokos, T. Bountis and C. Antonopoulos, Physica D **231**, 30 (2007).

[50] T. M. Rocha Filho and B. Marcos, In preparation.